

New insights into Photochromic Properties of *N*-Salicylideneaniline Derivatives Using a CoCrystal Engineering Approach

Gabriel M. Mercier^a, *Koen Robeyns*^a, *Nikolay Tumanov*^b, *Benoit Champagne*^b, *Johan Wouters*^b, *Tom Leyssens*^{a*}

^a Institute of Condensed Matter and Nanosciences, Université catholique de Louvain, 1348 Louvain-la-Neuve, Belgium

^b Unité de Chimie Physique Théorique et Structurale, Chemistry Department, Namur Institute of Structured Matter (NISM), University of Namur, 61 rue de Bruxelles, B-5000 Namur, Belgium

* Corresponding author: tom.leyssens@uclouvain.be

Keywords

N-Salicylideneaniline, anil, photochromism, crystal engineering, cocrystal screening, Diffuse Reflectance Spectroscopy.

Abstract

In this contribution, we aim to modify the photochromic properties of anils using a crystal engineering approach. Previous work has shown cocrystallization to alter the photochromic behavior of anils. Here a full screening of 15 anil derivatives (including 8 newly described anils) with 21 coformers (carboxylic acids, amides and halogenated benzene derivatives) was performed, resulting in 89 new anil cocrystals. This large amount of results allows drawing statistically valid insights on the complex photochromic mechanism ~~providing evidences~~ of a continuous phenomenon instead of the classic binary photochromic/non-photochromic~~s~~ one. This is supported by the discovery of “weakly photochromic compounds” presented in this contribution. All the results ~~presented here~~ allowed ~~us to confirm~~ confirming that an enol-imine character is a requirement and that reducing the amount of short contacts involving the moieties of interest is an interesting way to fine-tune properties as ~~it this~~ acts on both electronical and structural aspects. ~~Going along with that~~ Following this “continuous hypothesis”, the role of the dihedral angle has been explored and shown to be related to the intensity of photochromism ~~instead of being determinant for its occurrence~~. On top, in this contribution we present a novel way of interpreting DRS (Diffuse Reflectance Spectroscopy) data.

Introduction

Photochromism, defined as a light induced reversible color change of a material [1] is a property of continuous interest as it serves for many applications such as: optical devices [2,3], intelligent screens [4], changing color lenses [5], secured inks for banknotes or confidential notes [6,7] and optical data storage [8,9].

Among photochromic materials *N*-SalicylideneAniline (anil) derivatives are among the most studied as they present this property at the solid-state, showing high solid-state stability [10] and easy synthesis [11,12].

Anil photochromism is attributed to a *cis-trans* isomerization mechanism as illustrated in Figure 1. At room temperature, most anils present an enol /*cis*-keto equilibrium usually in favor of the enol form. This equilibrium involves an internal proton transfer between the nitrogen of the azomethine bond and the oxygen of the ortho-phenolic moiety. A change in temperature shifts the equilibrium to the *cis*-keto form, associated with a change in color from white (enol) to yellow (*cis*-keto). Upon UV-*vis* irradiation, both enol and *cis*-keto form can undergo a transition to a *trans*-keto form [3,11-18]. As this latter absorbs at higher wavelengths, this “photochromic” transition is clearly visible with the solid usually presenting a color change from colorless/yellow to red. Even if many anils are photochromic in solution [19], only a limited number of them present this feature in the solid state.

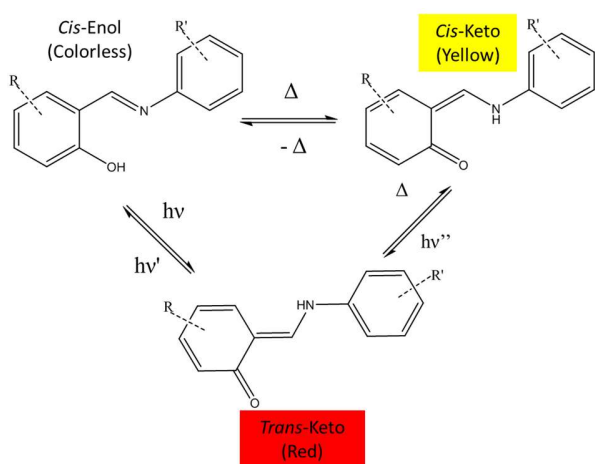


Figure 1: general scheme of the main thermo- and photochromic transitions in anils.

To understand why at the solid state some anils are photochromic and others not, early studies tried to link the photochromic characteristic to structural features, mainly focusing on the dihedral angle present between the aromatic moieties. Indeed, most of the photochromic anils reported show a dihedral angle $\varphi > 25^\circ$ [18,20-22] while planar anils usually tend to be thermochromic only [23]. However, recent findings disclosed this feature is no longer sufficient, with increasing counter-examples appearing in literature [19]. The full structural environment of an anil does nevertheless have an important impact on its photochromism as shown by alteration of the properties when inserting anils in environments such as a polymers [21], Metal-Organic Frameworks (MOFs) [24,25], zeolites [26] or through a cocrystallization approach [27-29]. All of these studies combined with a theoretical study [22] highlight the necessity of an open-packing structure to be a prerequisite for photochromism (presence of an interplanar distance of at least 3.3 Å between molecular planes) [14,30].

Even though an open-packing is a requirement, it is not a guarantee for photochromism. A full understanding of why some anils are photochromic and others are not remains an open question. Such an understanding can help guide future synthetic efforts for novel photochromic materials, and furthermore will allow transforming non-respondent anils into photochromically active ones by changing structural surroundings [28]. Cocrystallization might be the most promising approach to perform such studies, as it is commonly applied to modify and improve the chemical and physical properties of pharmaceutical compounds [31-33]. This approach has already been used in the context of Schiff bases (to which anils belong [15]) and specifically in the case of *N*-Salicylideneaniline derivatives through hydrogen bonding [27-29] which recently provided a successful way to reversibly switch properties through hydration/dehydration [34] or through

ammoniation/deammoniation in case of salts [35]. Another recent approach used halogen bonding [36,37] ~~again proving the abilitas a tooly~~ to change photochromical properties.

In order to gain new insights into the link between photochromic activity and structural features, we performed a statistical study on a full set of anils as well as their cocrystals. By considering 15 different anils and coupling them to 21 cofomers, a substantial dataset is obtained with a variety of different structural environments for a limited set of target compounds. This data underlines cocrystal screening efficiency for anils, and allows linking structural features to the photochromic characteristics. Furthermore we were able to show that each non-photochromic anil could be ‘switched on’ using a cocrystallization approach, highlighting the fact that, in principle, all anils can become photochromic in the solid state when given the right structural surroundings. ~~From this dataset we could-were able to explore-place many hypotheses/results already advancedpresent in litterature in perspective over-such asthe-structure-property relationship the -such-has~~ keto-enol equilibrium, dihedral angle, free space and short contacts confirming the importance of these last ones over the ortho-hydroxy moiety [19] but also with the moving moiety which is a new conclusion to the best of our knowledge.

Experimental Section

Starting Materials and Synthesis of the different anils are described in the supporting information (section 10).

Mechanochemical Cocrystal Screening. Liquid-assisted grinding (10 μ l of acetonitrile) was performed using an equimolar ($\pm 10^{-3}$ mol) mixture of starting materials. Samples were ground in a RETSCH Mixer Mill MM 400 for 90 min with a beating frequency of 30 Hz. The resulting powders were characterized using X-ray Powder Diffraction. Upon cocrystal identification,

attempts were made to obtain a single crystal of suitable size and quality for X-RD single crystal measurement. As chemical reactions can occur during liquid-assisted grinding, ¹H-NMR was used to eliminate samples that led to degradation/reaction.

Single Crystal Formation. Solvent evaporation at room temperature starting from an under-saturated solution, yielded single crystals of suitable quality for: **C-C16**, **D-C1**, **E**, **E-C1**, **E-C2**, **E-C4**, **E-C5**, **E-C6**, **E-C8**, **E-C8**, **E-C9**, **E-C11**, **E-C12** (solvate), **F-C4** (hydrate), **F-C5**, **H**, **I-C10** (hydrate), **L** (hydrate), **M**, **M-C15**, **N**, **N-C5** (hydrate), **O-C13** from acetonitrile; for **C-C20** from ethanol; for **D** from acetone; and for **F-C9** from ethyl-acetate.

Saturated solutions were prepared by adding an excess of compound to acetonitrile. By combining equivalent supernatant volumes of target anil and coformer and leaving this combined solution to evaporate at room temperature single crystals were obtained for **A-C20**, a monohydrate of **D** (from the experiment coupling anil **D** and coformer C2), a dihydrate structure of **E** (from the experiment coupling anil **E** and coformer C13) for anil **G** (from the experiment coupling anil **G** and coformer C3) and for anil **H** (from the experiment coupling anil **H** and coformer C9).

X-Ray Powder Diffraction (XRPD). X-ray diffraction measurements were performed on a Siemens D5000 diffractometer equipped with a Cu X-ray source operating at 40 kV and 40 mA and a secondary monochromator allowing to select the K α radiation of Cu ($\lambda=1.5418$ Å). A 2 θ scanning range from 2° to 50° at a scan rate of 0.6° min⁻¹ was applied. Simulated patterns of the known starting compounds were calculated from their single crystal structures with Mercury 3.5.1 and plotted with WinPLOTR (version: September 2015). For each reported mixture the diffraction pattern (in blue) is superimposed onto simulated patterns of its components (in red for

the corresponding anil and green for the co-former). All data are normalized to 100 for the highest peak. We assume formation of new phases when at least 2 new peaks appear and at least 2 reference peaks are missing.

Single Crystal X-Ray Diffraction. Structures were integrated with the CrysAlisPro software [38] and the implemented multi-scan absorption correction procedure was applied. Each structure was solved by direct methods, SHELXT [39] and refined by full-matrix least squares on $|F|^2$ using SHELXL-2014 or 2018 [40] Non-hydrogen atoms were refined anisotropically and hydrogen atoms were either placed on calculated positions in riding mode with temperature factors fixed at 1.2 times U_{eq} of the parent atoms and 1.5 times U_{eq} for methyl groups, or located in the Fourier difference maps when involved in H-bonds.

Diffuse Reflectance Spectroscopy Measurements. DRS spectra were obtained with a Varian 5E spectrophotometer equipped with a “praying mantis” diffuse reflection accessory and were converted to absorption spectra using the Kubelka-Munk function [41,42] and using PTFE as a reference for baseline correction. Spectra were measured on pure solid and were normalized relatively to their highest peak. Signal assignment was supported by reported band range for *N*-Salicylideneaniline derivatives [43].

~~Before~~ Prior to the DRS measurement, the purity of the new solid phase was checked through XRPD patterns to ensure results belongs to the the cocrystal phase is the only phase present, and the measurement does not suffer interference from one of the co-crystal and not to parent compounds. DRS results showing show an important shift of the trans-keto band (CFR Table 2) which also confirmed inherently confirms the presence of a new phase.

A novel alternative way of looking at the DRS data is presented here. Photochromic profiles are obtained by plotting the ratio of the spectra after/before irradiation. According to Kubelka-

Munk theory, the Kubelka-Munk function $F(R) = k/s$ where R is the reflectance, k is the molar extinction coefficient from the UV-Vis measurements in solution and s a scattering coefficient depending on all physical parameters of the sample surface [41,44]. If one assumes each existing electronic state (noted $\xi_i(T,\lambda)$ with λ the probe wavelength) to contribute to k , then k is dependent on the population $N_i(T)$ of these states and thus one can write: $k(\lambda) = \sum_i N_i(T) \cdot \xi_i(T,\lambda)$. The ratio of consecutive solid state measurements m and n (with conservation of the sample surface throughout the experiment) would give for a given wavelength: $F_m(\lambda)/F_n(\lambda) = \sum_i N_{im}(T) \cdot \xi_i(T,\lambda) / \sum_{in} N_{in}(T) \cdot \xi_i(T,\lambda)$ under the assumption that the scattering coefficient s does not change. For a given wavelength and temperature, this ratio changes upon irradiation, if a change in population of absorbing species occurs. If no population change occurs, or the species do not respond at a given wavelength, a fixed ratio is obtained. The ratio can therefore be directly related to population changes independently of experimental parameters such as surface, scattering coefficient or powder grain-size. Under the assumption that only a limited amount of absorbing species are present, non-photochromical compounds should present a perfectly linear profile (i.e. no evolution of state populations) equal to 1 (in case there is no experimental variation) while photo-respondent compounds should present upward and/or downward peaks as the state-population changes. In the context of this work, a change in ratio was considered significant when larger than ≥ 0.3 (30% intensity variation occurring over less than 50 nm). This value was chosen as experimental variations between consecutive measurements on a single sample were 10% (ratio change = 0.1) in the worst case. Considering 3 times this value, any change in ratio should represent a true population change. The highest ratio change is noted I_{\max} (in case of downward peak the ratio is inverted to have a clear comparison with normal cases). We then introduced $\Delta = F(R)_j - F(R)_i$, the absorption intensity difference between irradiated and non-

irradiated compound (from normalized Kubelka-Munk measurements) at the wavelength where the ratio is highest. We found that Δ values below 0.25 were not visible anymore by the naked eye.

Light irradiations were carried out with a MAX-303 lamp (Xenon light source 300 W) at 360 nm (by the use of 20 nm bandpass filters) for 30 minutes. Kubelka-Munk spectra were averaged over three measurements (removing and replacing the sample from the device between each but without changing the surface).

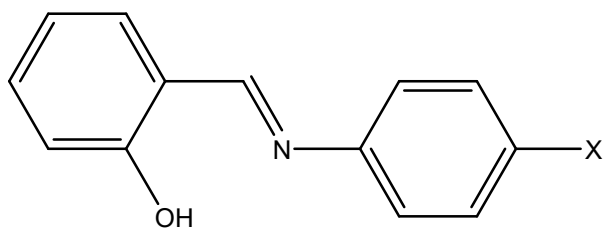
Thermal fading was analyzed by monitoring the evolution of absorption at 550 nm after irradiation (absorption measured each second over 6000 sec in a dark environment).

Short Contacts Analysis. We measured the total amount of close contacts involving any atom of a moiety of interest (detailed in the text) within a defined distance D , allowing quantifying weak, medium and strong short contacts. Thus we assigned a strong short contact when this contact is shorter than the sum of the Vander Waals radii of involved atoms (noted as $\sum r_{vdw}$, with values as defined in Mercury version 3.5.1) reduced by 0.05 Å ($D < \sum r_{vdw} - 0.05$ Å). A medium short contact is considered for lengths comprised between $\sum r_{vdw} - 0.05$ Å and $\sum r_{vdw} + 0.05$ Å and a weak short contact for a length comprised between $\sum r_{vdw} + 0.05$ Å and $\sum r_{vdw} + 0.2$ Å. Hirshfeld surfaces and 2D molecular fingerprints were calculated and drawn using the D_{norm} function of CrystalExplorer 17.5 Software [45] and corresponding CIF files.

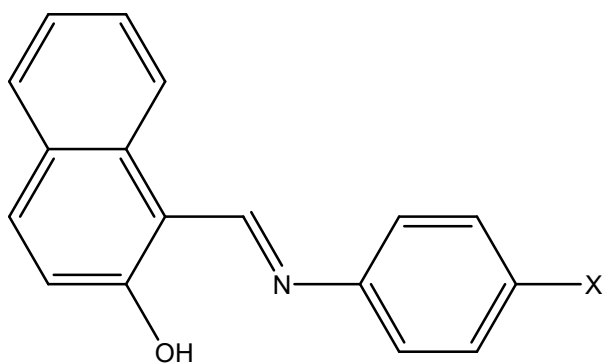
Results

Cocrystal screening.

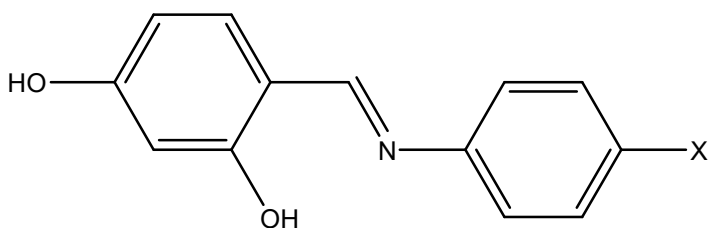
Scheme 1 shows the fifteen anil derivatives used (**A** to **O**) (see supporting information-section 10 for their synthesis) and Scheme 2 the selected 21 cofomers (C1 to C21), among which carboxylic acids, amides and halogenated benzene derivatives. Table 1 shows the results of the full cocrystal screening between anils and cofomers. For 33 combinations degradation of the anil occurred upon grinding.



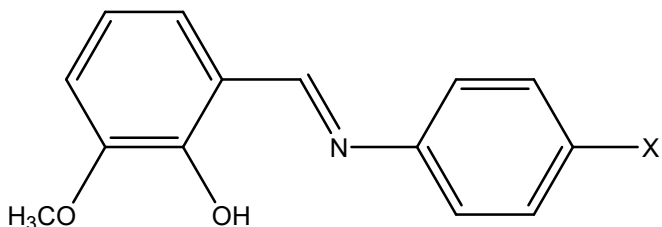
A: X=H
 B: X=F
 C: X=COOH
 D: X=CONH₂



E: X=H
 F: X=F
 G: X=COOH
 H: X=CONH₂

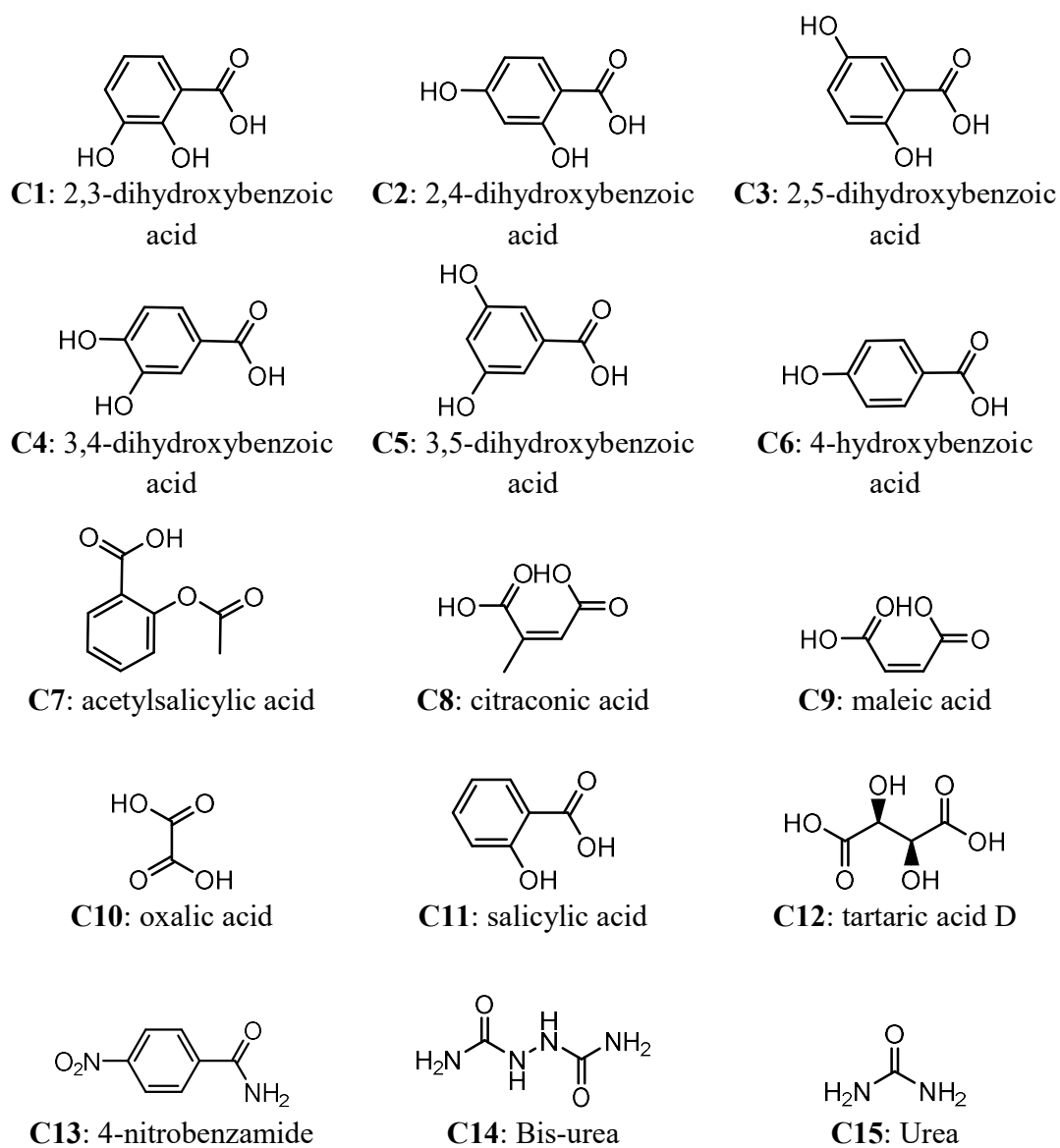


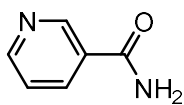
I: X=H
 J: X=F
 K: X=COOH
 L: X=CONH₂



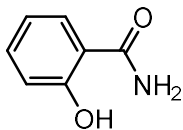
M: X=H
 N: X=F
 O: X=COOH

Scheme 1: anils studied in this work.

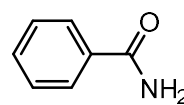




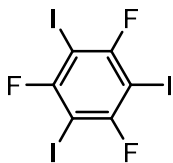
C16: Nicotinamide



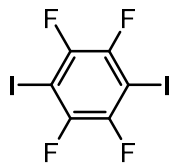
C17: Salicylamide



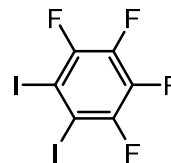
C18: Benzamide



C19: 1,3,5-trifluoro-2,4,6-triiodo-benzene



C20: 1,4-diiido-2,3,5,6-tetrafluoro-benzene



C21: 1,2-diiido-3,4,5,6-tetrafluoro-benzene

Scheme 2: cofomers selected for the cocrystal screen.

Table 1 shows a total of 95 cocrystals identified out of 315 possible combinations, 21 of which were structurally analyzed. This corresponds to a cocrystal formation successrate of +/- 30%. Even though such high rates are occasionally observed in literature [46] the generally accepted success rate is about 10 to 15% [44,47]. The high number observed here is likely due to the co-former selection, as we focused on co-formers already prove to cocrystallize with anils [28,29]. The efficiency of carboxylic acids as co-formers is apparent from Table 2 and is likely due to the possibility of forming hydrogen bonds between the carboxylic acid of the cofomer and the anil –OH bond. It is also apparent from the table 1 that the second and third anil series (respectively with the naphthyl and para hydroxy group on the salicylidene moiety) have an enhanced tendency to form cocrystals. This can also be explained by intermolecular interactions such as $\pi \cdots \pi$ interactions or hydrogen bonding with the –OH group.

Table 1: Cocrystal screening results. Deg. = degradation. CC = cocrystal formation and CC-SC = cocrystal which is structurally characterized. Empty cell = no cocrystal observed.

	A	B	C	D	E	F	G	H	I	J	K	L	M	N	O
C1				CC-SC	CC-SC	CC		CC		CC					
C2	Deg. ^a	CC ^a		CC	CC-SC		CC	CC							
C3					CC	Deg.	CC	CC			CC				
C4	Deg. ^a	CC ^a	CC		CC-SC	CC-SC		CC	Deg.	Deg.	CC		Deg.		
C5			CC	CC	CC-SC	CC-SC	CC				CC		CC	CC-SC	Deg.
C6					CC-SC	CC	CC	CC		CC	CC				Deg.
C7									CC	CC	Deg.				
C8	CC-SC ^a	Deg. ^a	CC	Deg.	CC-SC	CC	Deg.	Deg.	CC	CC	Deg.		Deg.	Deg.	Deg.
C9	Deg. ^a	CC ^a	CC	Deg.	CC-SC	CC-SC	Deg.	Deg.	CC	CC	CC	Deg.			CC
C10	Deg. ^a	CC ^a	CC	Deg.	CC	CC	Deg.	Deg.	CC-SC	CC	CC	Deg.	CC	CC	
C11				CC	CC-SC	CC			CC	CC					
C12				Deg.	CC-SC	CC		CC	CC			CC			
C13					CC		CC								CC-SC
C14								Deg.							
C15					CC						CC		CC-SC		CC
C16			CC-SC				CC	CC		Deg.	CC				CC
C17							CC								CC
C18															
C19					CC	CC		Deg.							
C20	CC-SC ^b		CC-SC	CC	CC			Deg.					CC		CC
C21					CC	CC	CC	Deg.						CC	

^a Results from previous work [28]

^b Result published by A. Carletta et al. [36]

Photo- and non-photochromic behavior

All cocrystals as well as all parent anils were irradiated at 365 nm for 30 minutes and their solid state absorption spectra were recorded. DRS strongly depends on experimental parameters such as surface planarity, grain-size, sample holder position, etc. [41], as illustrated in Figure 2 (left). An absolute variation up to 10% is not rare between two consecutive measurements, even when leaving the sample holder and sample in place. We thus decided to treat the data as mentioned above, coming to a signal that is less parameter dependent (Figure 2 - right).

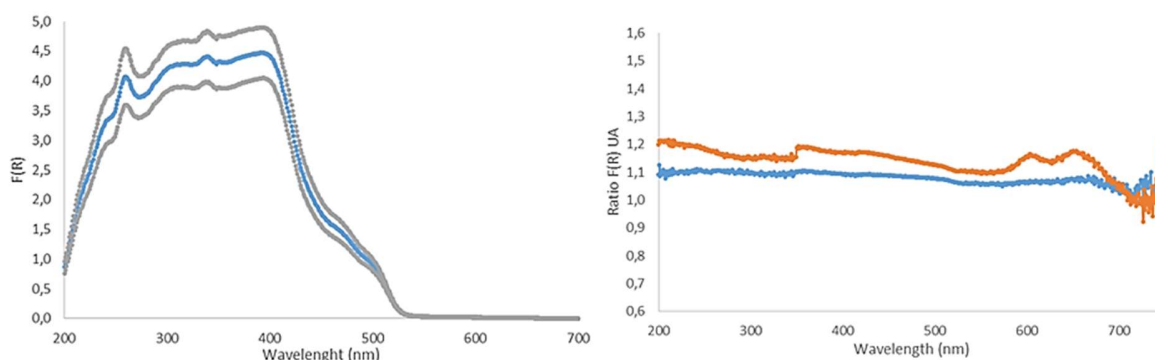


Figure 2 (left): Averaged DRS (Kulbelka-Munk) measurements of anil **B** (blue curve) over 8 measurements, with ± 1 standard deviation (grey curves). (Right): ratio of two consecutive measurements (blue curve) and ratio of 1st and 8th measurement (orange curve) for anil **B**.

As mentioned above, this relative signal shows upwards and downwards peaks when irradiation leads to population changes of different forms. This is illustrated in Figure 3, showing the DRS spectra for the A-C20 (photochromic) and C-C4 (non-photochromic) cocrystals, as well as the relative signal of the spectra before and after irradiation. The non-photochromic cocrystal show a flat line for all wavelengths, while a positive peak is observed when the cocrystal is photo-responsive, with a population increase of the *trans*-keto form as shown by the positive peak at around 560 nm. The value of the maximum ratio is further defined as I_{\max} .

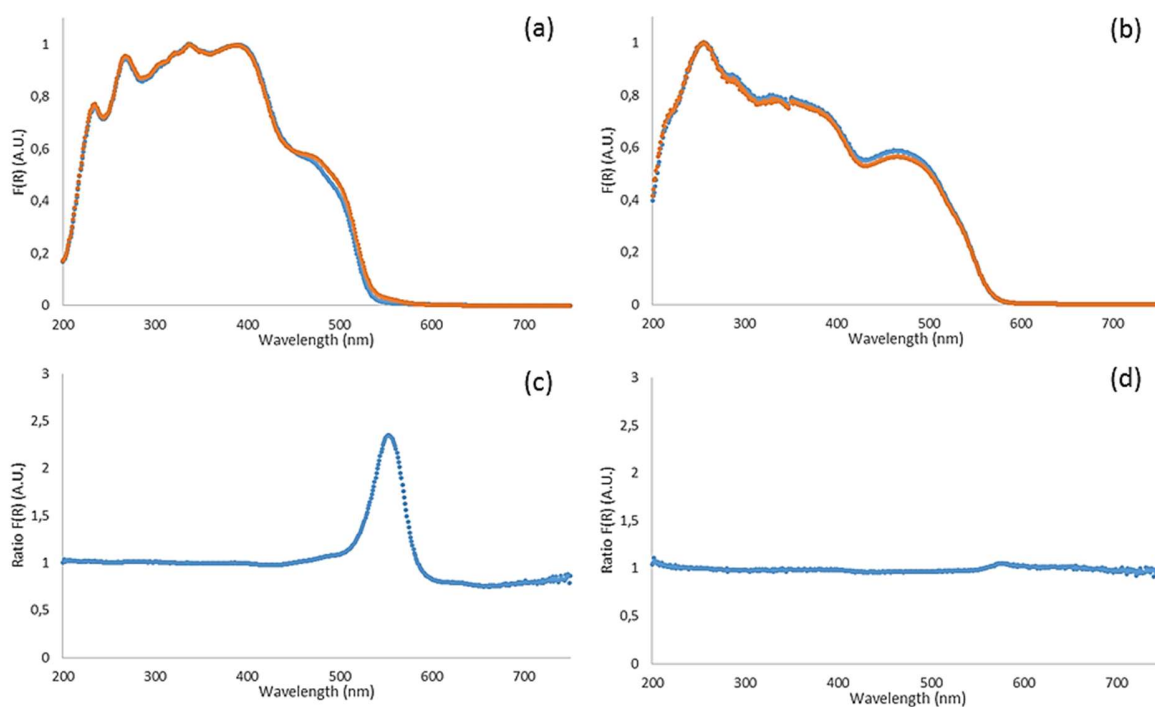


Figure 3: Normalized DRS spectra of cocrystals (a) A-C20 and (b) C-C4. Spectra before (blue) and after (orange) irradiation at 360 nm. Relative ratio of both spectra for cocrystal A-C20 (c) and C-C4 (d).

This result is also confirmed visually (Figure 4), with cocrystal A-C20 showing a weak but visible color change (from yellow to orange).

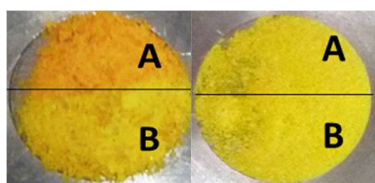


Figure 4: compounds A-C20 (left) and C-C4 (right). Top part (A) has been irradiated at 360 nm for 30 minutes while bottom part (B) was masked during the irradiation.

Analysis of the signal ratio (appearance of a peak at +/- 600 nm upon irradiation at 360 nm) allowed identifying 5 photochromic anils: **A**, **C**, **D**, **M** and **O**, with anil **A** and **C** already been reported as such [48,49]. Among the 95 cocrystals 20 were found photochromic: **A-C20**, **B-C4**, **B-C9**, **B-C10**, **B-C20**, **C-C8**, **C-C16**, **C-C20**, **C-C21**, **D-C2**, **D-C5**, **E-C15**, **H-C1**, **H-C16**, **I-C7**, **I-C12**, **J-C6**, **J-C7**, **M-C15** and **O-C15**. It is interesting to highlight that **B-C4**, **B-C9** and **B-C10** were previously reported as non-photochromic [28]. This is understandable as the peak height is around 1.3 (the lower limit used in this work). Furthermore, calculating the absorption difference Δ (as detailed in experimental part) we found a $\Delta \approx 0.05\%$, an extremely low value (not detectable by the naked eye) which explains they were reported non-photochromic. The data treatment presented in this paper can therefore help to identify borderline cases (Figure 5). The presence itself of borderline cases is new and shows photochromism to be a continuous phenomenon instead of a binary one, as the limit between photochromic and non-photochromic character is hard to find and has been established here based on experimental limitations (see experimental part) more than on an explicative model.

All the compounds presented here completely faded under visible light and some interesting cases were studied further (see Kinetic paragraphs below).



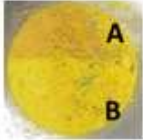
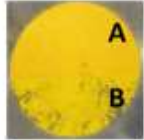

A-C20	M-C15	J-C7	C-C16	D-C5
				
$\Delta \approx 5\%$	$\Delta \approx 2.4\%$	$\Delta \approx 2\%$	$\Delta \approx 0.7\%$	$\Delta \approx 0.25\%$

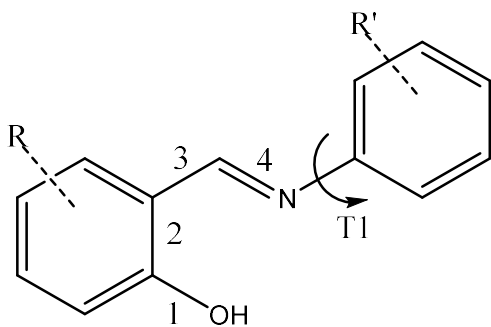
Figure 5: Comparison of not-irradiated (Bottom part - B) and irradiated (Top part - A) materials for different delta values/different cocrystals. As delta decreases it is harder to distinguish the color change.

Table 1 (combined with DRS-ratio analysis) also reveals that most of anils considered in this work lead to both photochromic as well as non-photochromic cocrystals. This also implies that for all parent compounds which are non-photochromic (**B**, **E**, **F**, **H** and **I**) cocrystallization can always be used as a tool to render them photochromic. Similarly, all photochromic anils (**C**, **D**, **M**, **O**) can be ‘turned off’ using this tool.

Linking photochromism to structural characteristics

Among the 110 forms identified (95 cocrystals and 15 parent anils), 8 photochromic ones were structurally characterized (**A** [48], **C** [27], **D**, **M** [50], **A-C20** [36], **C-C16**, **C-C20** and **M-C15**). The structural data and ORTEP representations of the ones determined here can be found in the supporting information (section 9).

Table 2 reports the main structural features of the photochromic center (Scheme 3), the maximum ratio change I_{\max} and the intermolecular distances: distance between parallel planes (Figure 6) for structures presenting a “close-packing” feature.



Scheme 3: Reference diagram with the bond lengths of interest marked as 1 to 4 and the main dihedral angle T1 (between the two aromatic rings).

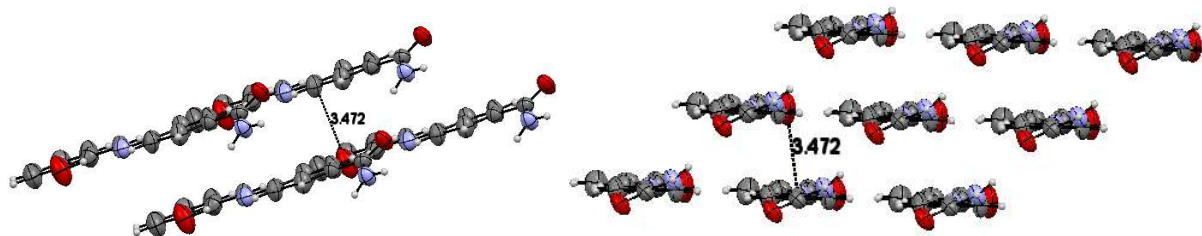


Figure 6: Interplanar distance illustrated in case of anil **D** along two different views.

Table 2: Main structural data of photochromic solids, as well as maximum ratio intensity (and its corresponding wavelength). Novel structures are highlighted in green.

Compound	Bond 1 (Å)	Bond 2 (Å)	Bond 3 (Å)	Bond 4 (Å)	T1 Angle (°)	I_{\max} (A.U.) (λ nm)	Interplanar Distances (Å)
A ^a	1.352	1.419	1.455	1.280	47(2)	45 (535 nm)	/
C ^a	1.345	1.391	1.446	1.276	6.4(4)	9.3 (572 nm)	3.420
C-C16	1.359(8)	1.369(8)	1.435(8)	1.296(7)	12(2)	2.2 (560 nm)	3.424
C-C20	1.347(5)	1.406(6)	1.465(5)	1.283(5)	5.6(2)	1.6 (569 nm)	3.462
D	1.344(2)	1.384(3)	1.449(3)	1.268(2)	0.6(5)	1.6 (571 nm)	3.472
M ^a	1.356(2)	1.406(2)	1.449(3)	1.284(2)	30(2)	3.1 (578 nm)	/
M-C15 ^b	1.347(4)	1.397(7)	1.445(9)	1.282(5)	26.4(2)	2.1 (587 nm)	/
X₁ ^a	1.350(3)	1.400(3)	1.444(3)	1.284(3)	30(3)	6 (550 nm)	3.597
X₂ ^a	1.350(2)	1.403(3)	1.446(3)	1.281(3)	39(2)	16 (555 nm)	3.275
X₃ ^a	1.346(2)	1.402(2)	1.446(2)	1.281(2)	30(3)	7 (575 nm)	3.533
Average	1.350	1.398	1.448	1.282	23	/	/
Standard deviation	0.005	0.014	0.008	0.007	16	/	/

^a Compound **A**, **C** and **M** from respective refs [48], [27] and [50]. **X₁**, **X₂**, **X₃** are taken from [29]

^b Cocrystal **M-C15** presents two slightly different molecules in the asymmetric unit. The results presented here are the average values.

Table 2 shows photochromic centers to have rather similar bond lengths as reflected by the small standard deviations. Based on reference bond lengths [28] the photochromically active compounds can be considered of the Enol-Imine type confirming previous studies [19]. All compounds (except **A**) were measured at room temperature proving a weak thermochromic character (as the thermal equilibrium is displaced toward keto form with increasing temperature). Interestingly, the values of the dihedral angle varies between 0 and 40°, with a strong standard deviation. The largest dihedral angle found in literature for a photochromic anil is 90° [51] while we here present a cocrystal C-C20 showing visible photochromism with a dihedral angle as low as 5.6°. In total, 4 photochromic compounds studied here presented a dihedral angle much lower than 25° as shown in table 2. Also 2 non-photochromic compounds presented a high dihedral angle of about 35° as shown in table 3 which means in total 6 over 28 compounds do not obey the “dihedral angle rule” in this contribution. Again the standard deviation is thus very important compared the average value for non-photochromic compounds. Another statistical study performed over a small dataset of 40 *N*-Salicylideneaniline derivatives still concludes to the importance of that this rule despite already a few the presence of counter-examples (6 over 40) [52]. These Our results confirms the recent believe that the dihedral angle (between the two aromatic rings) is not fully representative of the photochromic character, and the ‘dihedral angle rule’ ($\phi > 25^\circ$ is required for photochromism to occur) should therefore be revised [19,20].

Nevertheless, the value of the dihedral angle has a non-negligible impact on the photochromic process as it impacts the maximum ratio change observed upon irradiation. Figure 7 shows photochromic compounds with low dihedral angles (between 0° and 25°) to show only weak photochromic behavior whereas a stronger effect is obtained for the higher angles. This can possibly be explained by a loss of rigidity of the molecule in the solid with higher dihedral

angles, allowing an easier *cis/trans* isomerization [49]. The low ratio changes associated with the lower dihedral angle cases leads to visually difficult to observe color changes, and possibly explains why these anils could have been classified as non-photochromic. This would also explain how the dihedral angle rule came about. Thus we propose as a revision of this rule, proposin ~~that the dihedral angle should therefore relate~~ to relate to the intensity of the color change rather than to decide upon the photo- or non-photochromic character of the compound, and that leading to strong color changes for those photochromic compounds with $\phi > 25^\circ$ will exhibit intense color changes.

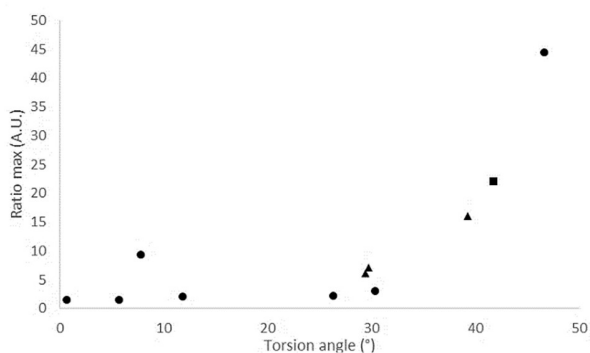


Figure 7: the maximum ratio change (arbitrary units) with respect to the absolute dihedral angle for 12 photochromic forms studied in this work (round dots) and those coming from literature (Ref. [29] - triangles and Ref. [3] - square).

Table 3: Structural data for non-photochromic solid forms – novel structures are highlighted in green.

Compounds E-C2, E-C4, E-C6 and O-C13 present two or more significantly different Anil forms in the asymmetric unit meaning averaging the values of bond lengths makes little sense. Values are then shown for each different form and noted with a small letter (a to d) at the end of compound's name. In case of E-C6, the second form is disordered and no accurate values can be

extracted from it. Along with compounds presented in Table 3, MeCN solvate of E-C12 and hydrates of D, I-C10¹, L and N-C5 were also found during the crystallization experiments but their simulated powder pattern did not match the initial powder pattern after grinding. They are thus discarded from discussion but their structures are displayed with the other CIF files in the supporting information. F-C4 hydrate perfectly matched the initial powder pattern and thus is conserved for further analysis.

Compound	Bond 1 (Å)	Bond 2 (Å)	Bond 3 (Å)	Bond 4 (Å)	Angle T1 (°)	Intermolecular distance (Å)
B ^a	1.352	1.410	1.448	1.275	6.3(1)	3.435
E	1.332(2)	1.408(2)	1.427(2)	1.297(2)	35(1)	/
D-C1	1.336(2)	1.414(2)	1.436(2)	1.291(2)	5.9(8)	3.367
E-C1 ^b	1.286(2)	1.434(4)	1.390(2)	1.314(5)	11(1)	3.518
E-C2a	1.283(5)	1.434(5)	1.401(5)	1.300(5)	10.1(6)	3.431
E-C2b	1.287(5)	1.432(5)	1.397(5)	1.315(5)	11.4(2)	3.607
E-C2c	1.329(6)	1.447(6)	1.377(6)	1.345(5)	0.90(2)	3.410
E-C2d	1.285(5)	1.428(6)	1.401(5)	1.313(5)	4(2)	3.326
E-C4 ^b	1.294(11)	1.436(11)	1.404(10)	1.312(11)	9(5)	3.321
E-C5a	1.331(6)	1.416(6)	1.400(6)	1.304(5)	7.3(8)	3.342
E-C5b	1.296(6)	1.427(6)	1.408(6)	1.315(6)	6.90(8)	3.342
E-C6a	1.293(5)	1.441(6)	1.388(5)	1.329(5)	3.2(8)	3.477
E-C6b	1.284(11)	1.398(11)	1.392(9)	1.326(10)	7.6(7)	3.270
E-C6c ^c	1.277(14)	1.402(14)	1.394(14)	1.325(15)	6(4)	3.270
E-C9 ^d	1.318(3)	1.412(3)	1.418(3)	1.302(3)	0.9(9)	3.495
E-C11 ^{b,c}	1.298(5)	1.44(3)	1.394(12)	1.316(12)	5(5)	3.477
F ^e	1.322(2)	1.409(2)	1.423(2)	1.296(2)	21(1)	3.412
F-C4	1.289(2)	1.430(2)	1.398(2)	1.308(2)	10(1)	3.524
F-C5 ^b	1.287(2)	1.427(2)	1.394(5)	1.310(5)	12(3)	3.258
F-C9	1.276(2)	1.437(2)	1.392(2)	1.317(2)	18.0(8)	3.389
G ^a	1.265	1.448	1.394	1.325	1	3.310
H	1.274(2)	1.438(3)	1.389(3)	1.315(2)	0.3(2)	3.440
N	1.342(2)	1.398(2)	1.441(3)	1.275(2)	12.4(6)	3.353
O-C13a	1.355(4)	1.397(5)	1.444(5)	1.284(5)	36(2)	3.516
O-C13b	1.364(4)	1.398(5)	1.447(5)	1.278(5)	38(1)	2.882
Averages	1.306	1.422	1.409	1.305	10.6	3.38
Standard deviations	0.027	0.015	0.020	0.015	10.2	0.14

^a Structure from CSD: CAVQAR02 [53] and DIWMAY [54] for Anils **B** and **G** respectively.

¹ I-C10 was observed as a cocrystal salt instead of pure cocrystal.

^b Average values of extremely similar structures in crystal packing. Errors displayed are the highest value between bond lengths error and calculated standard deviation on the average.

^c Structure is disordered so values are less accurate.

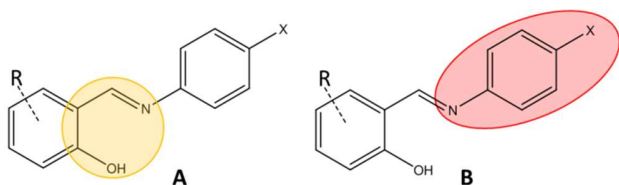
^d E-C9 was observed as a cocrystal salt.

^e Values used here are from a newly crystallized structure and not from MUDGAT [55] structure in CSD.

Table 3, in turn, reports the data for 20 non-photochromic compounds. With exception of **B**, **N** and **O-C13**, all the compounds present an enhanced keto character. This seems to suggest that a more pronounced keto form leads to a reduced possibility of photochromism **in accordance with** previously reported results [19]. In other words the enol-imine character can therefore be seen as a requirement for photochromism. However, as mentioned there are also some anils showing enol-character which are non-photochromic only, or which show both characteristics as eg. anil **C** [49]. On the other hand, no photochromic anil was identified showing an enhanced keto-character. One could therefore conclude that a partial keto-character (bond 1 < 1.34 Å) excludes photochromism while an enol-imine character is a necessary condition (but not a guarantee) for photochromism.

A further factor which is often mentioned in the context of photochromism is the presence of an open or close packing structure [11]. We therefore investigated whether an open packing is present in all photochromic anils (enol-imine character) and absent for the non-photochromic compounds. First of all it should be noted that all photochromic compounds show an interplanar distance of at least 3.3 Å, the limit for open packing according to literature [11]. However, all non-photochromic **studied here** also present this feature. The difference between open and closed packing on its own does therefore not seem a determining factor. Recent studies, indeed show a combination of different structural factors such as free available space, packing index and dihedral angle is likely required if one would aim at predicting photochromism [56,57]. In future

efforts, the open-packing feature could therefore still intervene when combined with other factors. To understand close-packing on a more fundamental level, short contacts were investigated. Short contacts are expected to block the movement of the anil and hence block the photochromic behavior. Through Hirshfeld surface analysis Wouters et al. already highlighted a link between the C \cdots C π -stacking interactions and the presence of photochromism [29]. As this type of interaction is correlated with the overall packing, studying short-contacts might therefore be a valid approach to increase the understanding of the structure-property relationship. We therefore focused first on the total number of short contacts involving any of the atoms of two sub-units of the anil: the “photochromic center” and the “moving phenyl moiety” as shown in scheme 4. These subunits are present in all cases considered here and are expected to be the most important with respect to the photochromic process. Short contacts were divided into three categories in order to rationalize the results: strong ($D < \sum r_{vdw} - 0.05 \text{ \AA}$), medium ($\sum r_{vdw} - 0.05 \text{ \AA} < D < \sum r_{vdw} + 0.2 \text{ \AA}$) and weak ($D > \sum r_{vdw} + 0.2 \text{ \AA}$). This analysis was performed on the 8 photochromic compounds and 20 non-photochromic compounds discussed here (see experimental section for detailed explanation and Supporting Information-section 13 for detailed results). A summary of this analysis is presented in Table 4 below.



Scheme 4: General anil skeleton with the 7 atoms of the “photochromic center” (A) circled in yellow and the 12 atoms of the “moving phenyl moiety” (B) circled in red.

Table 4: Average amount of strong, medium and weak short contacts for each moiety in function of the photochromic nature.

moiety	Nature of compounds	Strong	Medium	Weak	Total	Standard deviation
A	Photochromic	0.44	1.88	5.00	7.31	2.25
	Non-photo.	1.80	1.58	4.23	7.65	2.90
B	Photochromic	0.88	2.06	6.63	9.56	2.13
	Non-photo.	1.85	2.48	7.98	12.23	2.43

Table 4 shows some interesting overall features. The total cumulated average number of short contacts is significantly higher for the moving moiety of non-photochromic compounds (12.23 vs 9.56). One could therefore state that this moiety is in average more stabilized in non-photochromic compounds, impeding rotation around T1.

For the photochromic center there does not seem to be a major different in total amount of short contacts between the photochromic and non-photochromic compounds. However there is a significant difference in strong (shorter) close contacts: non-photochromic compounds show a four-fold increase in strong interactions (1.80 vs. 0.44). In depth analysis revealed that for the photochromic compounds, only 2 (25% of photochromic compounds studied here) present a strong short contact involving the hydroxy group of the photochromic center while this feature was observed for 18 (90% of non-photochromic compounds studied here) of the non-photochromic compounds. From these we can draw two conclusions: 1) the moving moiety (B) is more stabilized (more involved in all type of short contacts) for non-photochromic compounds; 2) for the photochromic center (A) there is an important difference in amount of strong short contacts between the photochromic and non-photochromic compounds meaning these strong short contacts might play a role in inactivating photochromism. As the majority of

these strong short contacts are in fact hydrogen bonding interactions (with the –OH group) they are able to shift the keto-enol equilibrium toward the keto form, thus increasing the energy-barrier to reach the *trans*-keto state and rendering the anils non-photochromic [19]. To illustrate this we decided to calculate Hirshfeld surfaces and 2D molecular fingerprints [58,59] for newly presented enol structures: C-C16, C-C20, **D**, **M** and **M-C15** along with **C** as reference for photochromic compounds and **D-C1**, **N** and **O-C13** along with **C** as reference for non-photochromic compounds (both **D-C1** and **E** are close to the enol form with bond 1 > 1.33 Å). Calculated Hirshfeld surfaces with D_{norm} functions are presented in Figure 8 and corresponding fingerprints in Figure 9. As shown by Figure 8, most of photochromic compounds don't have strong short contacts involving the ortho-hydroxy moiety of the photochromic center with the exception ~~for~~ of cocrystal **M-C15** (f) which shows ~~however~~ photochromism can still occurs when strong short contacts are not able to displace the keto-enol equilibrium. ~~Along with this we can notice~~ In parallel, non-photochromic structures more likely present strong interaction involving the moving moiety as in the case of **E** (h) and **N** (i)

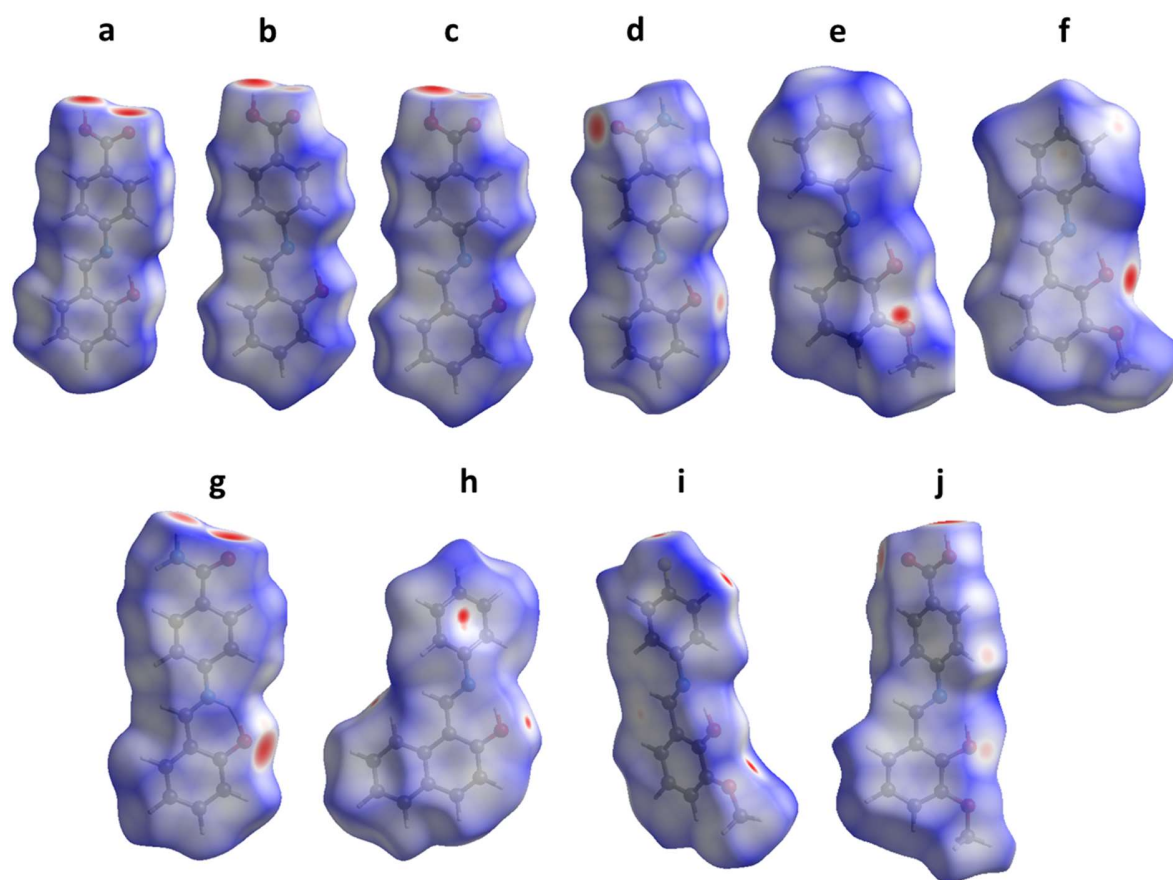


Figure [8]: Mapped Hirshfeld surfaces with D_{norm} functions for the anil moiety of photochromic compounds **C** (a), **C-C16** (b), **C-C20** (c), **D** (d), **M** (e), **M-C15** (f) and non-photochromic enol compounds **D-C1** (g), **E** (h), **N** (i) and **O-C13** (j). Red spots show strong intermolecular contacts, white spots show weak intermolecular contacts and blue spots show no intermolecular contacts.

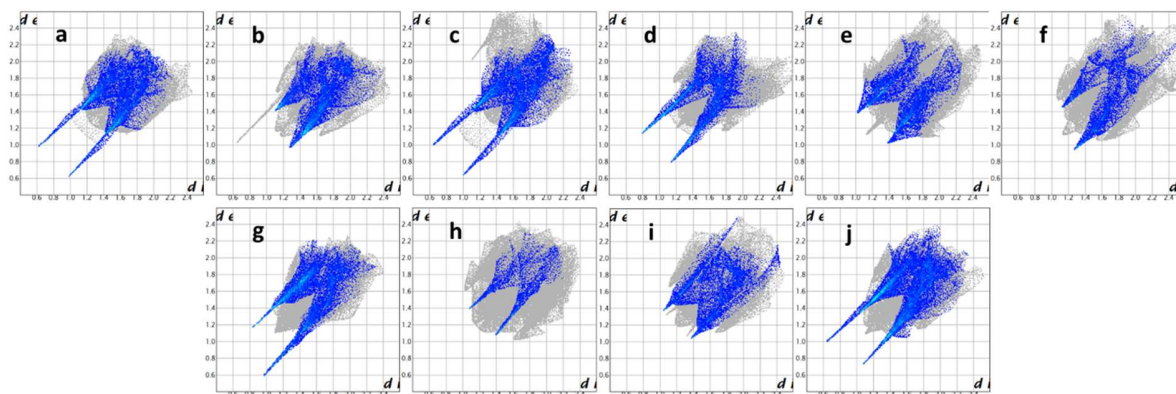


Figure [9]: Fingerprints of calculated Hirshfeld surfaces for the anil moiety of photochromic compounds **C** (a), **C-C16** (b), **C-C20** (c), **D** (d), **M** (e), **M-C15** (f) and non-photochromic enol compounds **D-C1** (g), **E** (h), **N** (i) and **O-C13** (j). Highlighted area corresponds to O...H interactions.

From the fingerprints (Figure 9) we can notice strong contributions to the O...H interactions in almost all cases. By comparison with Figure 8, we can assign ~~it~~-this to the carboxylic/amide or methoxy moiety for photochromic compounds **C** (a), **C-C16** (b), **C-C20** (c) and **M** (e) while in case of the non-photochromic compound **E** (h) and **N** (i) the only possible contribution is due to ortho-phenolic moiety. In the case of photochromic compounds **D** (d), **M-C15** (f) and non-photochromic cocrystal **D-C1** (g) and **O-C13** (j) both moieties contribute to the signal. The anil **D**/ cocrystal **D-C1** presents an interesting comparison of the impact of short-contacts on photochromism as anil **D** (d) exhibits weak photochromism and a weak contribution of the ortho-hydroxy group on Hirshfeld surfaces while cocrystal **D-C1** (g) shows a stronger contribution of this moiety with a complete removal of the photochromic behavior. Hirshfeld maps and fingerprints of other compounds (keto form) also exhibit strong short contacts involving the ortho-hydroxy moiety in most cases and are displayed in the supporting information, section 15. This result confirms previous studies over-on the impact of ~~that~~-this moiety/short contacts in

disabling photochromism [19] which means this can be used to fine-tune photochromical properties of anils: to promote photochromism in these compounds it is beneficial to reduce the number of short contacts in particular with two moieties of interest. For instance the addition of bulky groups on the anil might reduce the hydrogen bonds or π -stacking and T-axial interactions. This has already been successfully experimented (but in order to force a non-planar conformation - a complete different approach) by T. Kawato et al. [13]. They also performed the “Bulky-group substitution method” to increase the space available in order to allow the movement of the phenyl moiety [13] but which should also result in a global diminution of the amount of strong short-contacts and thus again show that engineering short-contacts aspects might be one-of-the key to fine-tune photochromism.

Kinetic measurements

In order to study further the impact of short-contacts, the thermal reversibility of photochromism of the cocrystals was studied focusing on two different photochromic systems, cocrystals A-C20 and C-C16, as for these compounds the respective parent anils A and C have already been studied [49,60].

The kinetic measurement was done at 550 nm which is close to the maximum ratio change for both compounds (respectively 556 nm and 558 nm) and presents an expected exponential decay over time after irradiation (disappearance of trans-keto band). The data was linearized and shows a two-stage first order kinetics for both cases, similar to reported behavior for anil C [13].

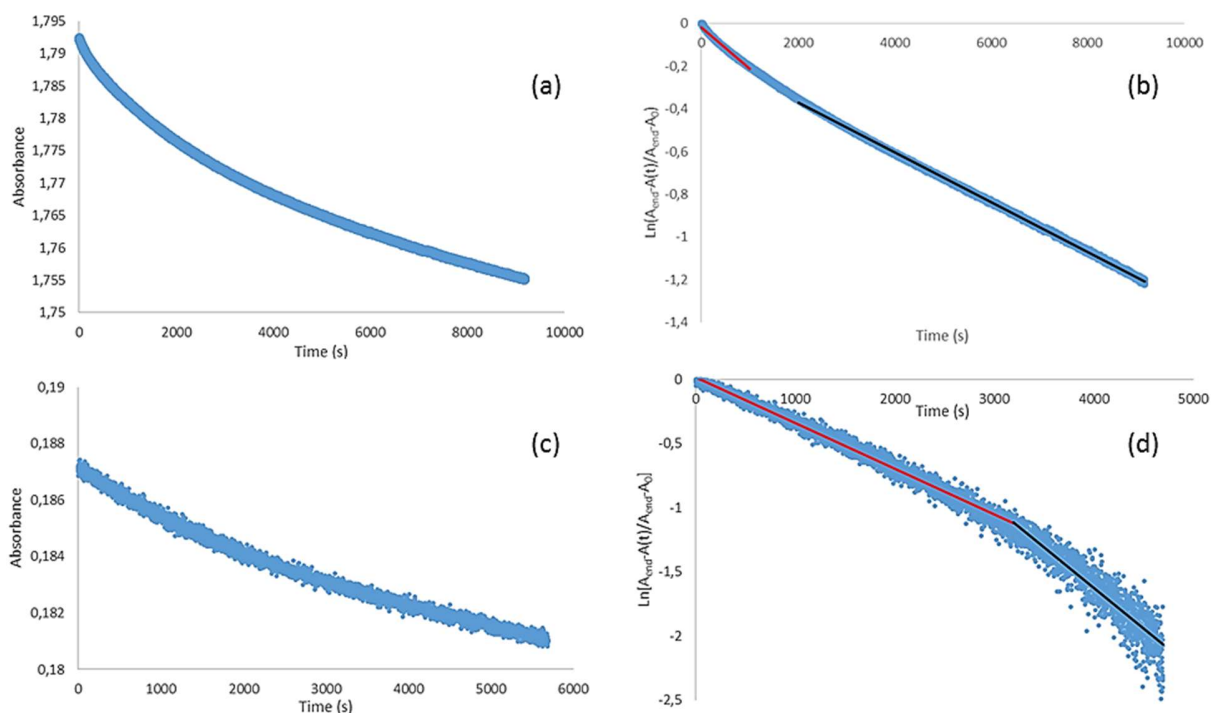


Figure 10: (a): Absorbance at 550 nm over time of A-C20 after irradiation at 365 nm. (b): First order linearization. (c): Absorbance at 550 nm over time of C-C16 after irradiation at 365 nm. (d): First order linearization.

The corresponding rate constants k_1 and k_2 were calculated using the Malkin equation $(\text{Ln}(\frac{\text{Abs}_\infty - \text{Abs}(t)}{\text{Abs}_\infty - \text{Abs}_0}) = -k.t)$ and yield values of $k_1 = 1.96 \times 10^{-4} \text{ s}^{-1}$ and $k_2 = 1.17 \times 10^{-4} \text{ s}^{-1}$ for A-C20 and for C-C16: $k_1 = 3.58 \times 10^{-4} \text{ s}^{-1}$ and $k_2 = 6.32 \times 10^{-4} \text{ s}^{-1}$. These latest values are of the same order of magnitude than those reported for anil C: $k_1 = 3.28 \times 10^{-4} \text{ s}^{-1}$ and $k_2 = 7.04 \times 10^{-4} \text{ s}^{-1}$ [49]. For anil A we measured a value of $k_1 = 3.57 \times 10^{-4} \text{ s}^{-1}$ at 20 °C while $k_1 = 1.4 \times 10^{-3} \text{ s}^{-1}$ is reported at 30 °C [60]). The usual reported range for k_1 in anils varies between $3 \times 10^{-2} \text{ s}^{-1}$ and $1.8 \times 10^{-8} \text{ s}^{-1}$ [2].

Cocrystallization in the case of compound **C** therefore almost shows no effect on the relaxation process. For anil **A** the rate constant (k_1) is about 2 times lower when **A** is inserted in the cocrystal. This can be correlated to the structure of these systems: both anil **C** and cocrystal **C-C16** have a similar interplanar distance (3.424 Å and 3.420 Å respectively for **C-C16** and **C**) and one intermolecular interaction ($O\cdots HC$ in both cases) directly involving the moving moiety. For the system with anil **A**, there are significant differences between the structure of anil and the cocrystal: in case of anil **A** there is no face-to-face orientation and only one (average-medium) T-Axial interaction $CH\cdots\pi$ while cocrystal **A-C20** presents an interplanar distance of 3.291 Å and two strong (short) $I\cdots\pi$ interactions involving the moving moiety. These features show the moving moiety is more stabilized in the cocrystal possibly explaining the slower relaxation.

Conclusion

Within this work 15 anils were screened with respect to 21 cocrystal formers, leading to 95 cocrystal systems. Carboxylic acids were found to be good cofomer candidates as a hydrogen bonding interaction with the anil $-OH$ group can be expected. Furthermore, we showed that cocrystallization can be used to ‘switch on’ any non-photochromic anil.

We also introduced a novel approach to the data interpretation by looking at the ratio of consecutive DRS measurements. This led to a better classification of photochromic and non-photochromic solids, allowing identifying those “weakly photochromic compounds” that do not (or barely) show a visible change when looking with the naked eye. Our data furthermore consolidates the current believe that the ‘dihedral angle rule’ should be revised, as the dihedral angle is not decisive for the photochromic nature of a compound, but rather impacts the intensity

of this effect. These results clearly suggest that photochromism is a continuous phenomenon and not a binary one.

Interestingly, all anils presenting a photochromic behavior at 360 nm showed a marked enol character at room temperature while non-photochromic (at 360 nm) compounds exhibited an enhanced keto-character. One can therefore conclude that a partial keto-character (bond $l < 1.34$ Å) excludes photochromism while enol-imine character is a necessary condition (but not a guarantee) for photochromism to occur at the working wavelength. Hydrogen bonding to the anil ortho-OH group can have a strong impact on the keto-enol character of a target compound and should be avoided as much as possible. Anils showing enol character but no photochromism show an important number of short contacts involving the moving moiety, and hence a likely reduced possibility of molecular movement (a requirement for photochromism). Overall this analysis thus confirms that to promote photochromism, intermolecular interactions should be reduced as much as possible, in alignment with the bulky substitution approach.

Supporting Information.

Structures described in this contribution have been deposited at the Cambridge Crystallographic Data Centre and allocated the deposition numbers CCDC 1903903 to 1903930. Supporting Information also contains XRPD, DRS spectra, $^1\text{H-NMR}$ Data, starting materials, thermal analysis (TGA/DSC), synthesis, structural chemical data and short contacts analysis of discussed compounds (PDF). This material is available free of charge via the Internet at <http://pubs.acs.org>.

Corresponding Author

* Email: tom.leyssens@uclouvain.be.

Acknowledgments. The authors would like to thank the UCL for financial support (Gabriel Mercier is a UCL teaching assistant). This work was published thanks to funding of "Actions de Recherche Concertées (ARC)" de la Direction générale de l'Enseignement non obligatoire et de la Recherche scientifique – Direction de la Recherche scientifique – Communauté française de Belgique. The authors would also like to Thanks Ir. Séverine Schiltz for her contribution to data processing through VBA coding.

References

- [1] G. H. Brown, Photochromism, Wiley-Interscience, New York **1971**.
- [2] K. Nakatani, J. A. Delaire, Reversible Photoswitching of Second-Order Nonlinear Optical Properties in an Organic Photochromic Crystal, *Chem. Mater.*, **1997**, 9, 2682-2684.
- [3] M. Sliwa, S. Létard, I. Malfant, M. Nierlich, P. G. Lacroix, T. Asahi, H. Masuhara, P. Yu, K. Nakatani, Design, Synthesis, Structural and Nonlinear Optical Properties of Photochromic Crystals: Toward Reversible Molecular Switches, *Chem. Mater.* **2005**, 17, 4727.
- [4] W. Zhu, Photochromic protective film and preparation method thereof Faming Zhuanli Shenqing, Patent **2015**, CN 105129225 A 20151209.
- [5] G. C. Yoo, Photochromic contact lens and manufacture method thereof, Repub. Korean Kongkae Taeho Kongbo, Patent **2018**, KR 2018137234 A 20181227.
- [6] M. Maurer, M. Huegin, T. Raimann, L. Feiler, B. Inderbitzin, A. Fuchs, Preparation of a photochromic ink, PCT Int. Appl., **2010**, WO 2010079098 A1 20100715.
- [7] D. Zhang, Photochromic anti-counterfeiting ink, Faming Zhuanli Shenqing, Patent **2016** CN 106147399 A 20161123.
- [8] B. L. Feringa, W. F. Jager and B. Delange, Organic materials for reversible optical data storage, *Tetrahedron* **1993**, 49, 8267-8310.
- [9] S. Kawata and Y. Kawata, Three-Dimensional Optical Data Storage Using Photochromic Materials, *Chem. Rev.* **2000**, 100, 1777-1788.
- [10] E. Hadjoudis, S. D. Chatziefthimiou, I. M. Mavridis, Anils: Photochromism by H-transfer, *Current Organic Chemistry*, **2009**, 13, 269-286.

- [11] E. Hadjoudis, *Molecular Engineering, Photochromic and Thermochromic Anils*, **1995**, 5, 301.
- [12] B. Kaitner, M. Zbačnik, Solvent-free Mechanochemistry of Two Thermochromic Schiff Bases, *Acta Chim. Slov.* **2012**, 59, 670.
- [13] K. Amimoto, T. Kawato, Photochromism of organic compounds in the crystal state, *Journal of Photochemistry and Photobiology*, **2005**, 6, 207-226.
- [14] F. Robert, A. D. Naik, F. Hidara, B. Tinant, R. Robiette, J. Wouters, Y. Garcia, Engineering Solid-State Molecular Switches: *N*-Salicylidene *N*-Heterocycle Derivatives, *European Journal of Organic Chemistry*, **2010**, 621–637.
- [15] B. C. Jain, P. Mirchandani, B. H. Iyer, P. C. Guha, Schiff's bases of 4-nitro-4'-aminodiphenyl sulfone and their reduction products, *Science and Culture*, **1946**, 11, 567-8.
- [16] M. D. Cohen, G. M. J. Schmidt, S. Flavian, Experiments on Photochromy and Thermochromy of Crystalline Anils of Xalicylaldehydes, *Journal of the Chemical Society*, **1964**, June, 2041-2051.
- [17] W. F. Richey, R. S. Becker, Spectroscopy and mechanisms of the photo- and thermal reactions of photochromic anil, *Journal of Chemical Physics*, **1968**, 49, 5, 2092-2101.
- [18] F. Milia, E. Hadjoudis, J. Seliger, Hydrogen Bond Studies In Thermochromic And Photochromic *N*-Salicylidene Anilines, *Journal of Molecular Structure*, **1988**, 177, 191-197.
- [19] M. S. Rawat, S. Mal, P. Singh, Photochromism in Anils - A Review, *Open Chemistry Journal*, **2015**, 2, 7-19.
- [20] S. D. Chatziefthimiou, Y. G. Lazarou, E. Hadjoudis, T. Dziembowska, I. M. Mavridis, Keto Forms of Salicylaldehyde Schiff Bases: Structural and Theoretical Aspects, *J. Phys. Chem.*, **2006**, 110, 23701-23709.
- [21] E. Hadjoudis, V. Verganlakis, C. Trapalis, G. Kordas, Environmental Effect of Sol-Gel Encapsulation on Photochromic and Thermochromic Anils, *Molecular Engineering*, **1999**, 8, 459-469.
- [22] F. Robert, A. D. Naik, B. Tinant, R. Robiette, Y. Garcia, Insights into the Origin of Solid-State Photochromism and Thermochromism of *N*-Salicylideneanils: The Intriguing Case of Aminopyridines, *Chem. Eur. J.*, **2009**, 4327-4342.
- [23] E. Hadjoudis, Solid State Photochromism of Anils, *Mol. Cryst. Liq. Cryst.* **1994**, 246, 127-134.

- [24] T. Haneda, M. Kawano, T. Kojima, M. Fujita, Thermo-to-Photo-Switching of the Chromic Behavior of Salicylideneanilines by Inclusion in a Porous Coordination Network, *Angew. Chem. internat. Edit.*, **2007**, 46, 6643-6645.
- [25] F. Robert, A. D. Naik, B. Tinant, Y. Garcia, *N*-Salicylidene anil anions as thermo-sensitive components of organic–inorganic hybrid materials, *Inorganica Chimica Acta*, **2012**, 380, 104-113.
- [26] I. Casades, M. Álvaro, H. García, M. N. Pillai, Photochemistry of anils in NaY zeolite, *Eur. J. Org. Chem.*, **2002**, 2074-2079.
- [27] K. Johmoto, A. Sekine, H. Uekusa, Photochromism Control of Salicylideneaniline Derivatives by Acid–Base Co-Crystallization, *Cryst. Growth Des.*, **2012**, 12, 4779-4786.
- [28] G. M. Mercier, K. Robeyns, T. Leyssens, Altering the Photochromic Properties of *N*-Salicylideneanilines Using a Co-Crystal Engineering Approach, *Cryst. Growth Des.*, **2016**, 16, 3198-3205.
- [29] A. Carletta, B. Xavier, T. Leyssens, B. Champagne, J. Wouters, Polymorphic and Isomorphic Cocrystals of a *N*-Salicylidene-3-aminopyridine with Dicarboxylic Acids: Tuning of Solid-State Photo and Thermochromism, *J. Phys. Chem. C*, **2016**, 120, 10001-10008.
- [30] E. Hadjoudis, I. M. Mavridis, Photochromism and thermochromism of Schiff bases in the solid state: structural aspects, *Chem. Soc. Rev.*, **2004**, 33, 579.
- [31] N. K. Duggirala, M. L. Perry, Ö. Almarsson, M. J. Zaworotko, Pharmaceutical Cocrystals: Along the Path to Improved Medicines., *Chem. Commun.*, **2016**, 52, 640–655.
- [32] N. Schultheiss, A. Newman, Pharmaceutical Cocrystals and Their Physicochemical Properties, *Cryst. Growth Des.*, **2009**, 9, 2950–2967.
- [33] A. Tilborg, B. Norberg, J. Wouters, Pharmaceutical Salts and Cocrystals Involving Amino Acids: A Brief Structural Overview of the State-of-Art, *Eur. J. Med. Chem.*, **2014**, 74, 411–426.
- [34] H. Sugiyama, K. Johmoto, A. Sekine, H. Uekusa, Reversible on/off switching of photochromic properties in *N*-salicylideneaniline co-crystals by heating and humidification, *CrystEngComm*, **2019**, 21, 3170-3175.
- [35] H. Sugiyama, K. Johmoto, A. Sekine, H. Uekusa, In-Situ Photochromism Switching with Crystal Jumping through the Deammoniation of *N*-Salicylideneaniline Ammonium Salt, *Cryst. Growth Des.*, **2019**, 19, 4324-4331.

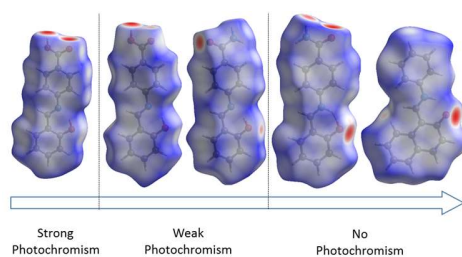
- [36] A. Carletta, M. Zbačnik, M. Vitković, N. Tumanov, V. Stilinović, J. Wouters, D. Cinčić, Halogen-bonded cocrystals of N-salicylidene Schiff bases and iodoperfluorinated benzenes: hydroxyl oxygen as a halogen bond acceptor, *CrystEngComm.*, **2018**, 20 (36), 5332-5339.
- [37] A. Carletta, M. Zbačnik, M. Van Gysel, M. Vitković, N. Tumanov, V. Stilinović, J. Wouters, D. Cinčić, Playing with Isomerism: Cocrystallization of Isomeric N-Salicylideneaminopyridines with Perfluorinated Compounds as Halogen Bond Donors and Its Impact on Photochromism, *Cryst. Growth Des.*, **2018**, 18, 6833–6842.
- [38] CrysAlys PRO, Data Collection and Processing Software for Agilent X-ray Diffractometers User Manual, Agilent Technologies UK Ltd., Oxford, UK, **2013**.
- [39] G. M. Sheldrick, SHELXT - Integrated space-group and crystal-structure determination, *Acta Crystallogr., Sect. A: Found. Crystallogr.*, **2015**, 71, 3-8.
- [40] G. M. Sheldrick, Crystal structure refinement with SHELXL, *Acta Crystallogr., Sect. C: Found. Crystallogr.*, **2015**, 71, 3-8.
- [41] J. Torrent, V. Barron, Diffuse Reflectance Spectroscopy, *Method of soil analysis. Part 5. Mineralogical Methods*, **2008**.
- [42] Advances in Catalysis, Chapter 3: Ultraviolet–Visible–Near Infrared Spectroscopy in Catalysis: Theory, Experiment, Analysis, and Application Under Reaction Conditions, B. C. Gates, H. Knozinger, Eds., F. C. Jentoft, Assoc. Ed., Elsevier, **2009**; Vol.52.
- [43] T. Fujiwara, J. Harada, K. Ogawa, Solid-State Thermochromism Studied by Variable-Temperature Diffuse Reflectance Spectroscopy. A New Perspective on the Chromism of Salicylideneanilines, *J. Phys. Chem.*, **2004**, 108, 4035-4038.
- [44] G. Kortuem, W. Braun, G. Herzog, Principles and methods of diffuse reflection spectroscopy, *Angew. Chem. internat. Edit.*, **1963**, 2, 7, 333-404.
- [45] M. J. Turner, J. J. McKinnon, S. K. Wolff, D. J. Grimwood, P. R. Spackman, D. Jayatila and M. A. Spackman, *CrystalExplorer17*, University of Western Australia, **2017**, <http://hirshfeldsurface.net>.
- [46] K. Fucke, S. A. Myz, T. P. Shakhtshneider, E. V. Boldyreva, U. J. Griesser, How good are the crystallisation methods for co-crystals? A comparative study of piroxicam, *New J. Chem.*, **2012**, 36, 1969-1977.
- [47] M. Viertelhaus, R. Hilfiker, F. Blatter, M. Neuburger, Piracetam Co-Crystals with OH-Group Functionalized Carboxylic Acids, *Cryst. Growth. Des.*, **2009**, 9, 2220-2228.
- [48] R. Destro, A. Gavezzotti, M. Simoneta, [Crystal structure of] salicylideneaniline, *Acta Crys. B*, **1978**, 34, 2867.

- [49] M. Avadanei, V. Cozan, S. Shova, J. A. Paixao, Solid state photochromism and thermochromism of two related *N*-salicylidene anilines, *Chemical Physics*, **2014**, 444, 43-51.
- [50] Y. Y. Yu, 6-Methoxy-2-[(*E*)-phenyliminomethyl]phenol, *Acta Cryst.*, **2011**, E67(4), o889.
- [51] M. Taneda, K. Amimoto, H. Koyama, T. Kawato, Photochromism of polymorphic 4,4'-methylenebis-(*N*-salicylidene-2,6-diisopropylaniline) crystals, *Org. Biomol. Chem.*, **2004**, 2, 499-504.
- [52] Multi-component crystals, Chapter 4: Control of photochromism in *N*-salicylideneaniline by crystal engineering, K. Johmoto, H. Uekusa, E. R. T. Tiekink (Eds.), J. Zukerman-Schpector (Eds.), De Gruyter, **2017**.
- [53] T.S. Chundawat, N. Sharma, P. Kumari, S. Bhagat, *Synlett*, **2016**, 27, 404-408.
- [54] M. Akkurt, S. O. Yildirim, A. M. Asiri, V. McKee, 4-[(2-Hydroxy-1-naphthyl) methylideneamino]benzoic acid, *Acta Cryst.*, **2008**, E64(4), o682.
- [55] H. Unver, D.M. Zengin, T. N. Durlu, *Anal. Sci.*, **2001**, 17, 1021-1022.
- [56] P.-L. Jacquemin, K. Robeyns, M. Devillers, Y. Garcia, Photochromism emergence in *N*-Salicylidene *p*-Aminobenzenesulfonate Diallylammonium Salts, *Chem. Eur. J.*, **2015**, 21, 6832-6845
- [57] H. Sugiyama, H. Uekusa, Relationship between crystal structures and photochromic properties of *N*-salicylideneaminopyridine derivatives, *CrystEngComm*, **2018**, 20, 2144-2151.
- [58] J. J. McKinnon, D. Jayatila, M. A. Spackman, Towards quantitative analysis of intermolecular interactions with Hirshfeld surfaces, *Chem. Commun.*, **2007**, 3814-3816.
- [59] M. A. Spackman, D. Jayatila, Hirshfeld Surface Analysis, *CrystEngComm*, **2009**, 11, 19-32.
- [60] H. Koyama, T. Kawato, H. Kanatomi, H. Matsushita and K. Yonetani, Utilization of crystal lattice cavities of host deoxycholic acid for achieving photochromism of guest salicylideneanilines in the crystal state, *J. Chem. Soc., Chem. Commun.*, **1994**, 579.

For Table of Contents Use Only

New insights into Photochromic Properties of *N*-Salicylideneaniline Derivatives Using a CoCrystal Engineering Approach

Gabriel M. Mercier, Koen Robeyns, Nikolay Tumanov, Benoit Champagne, Johan Wouters,
Tom Leysens.



New statistical insights into structure/photochromism relationship of *N*-Salicylideneaniline derivatives are presented here using a dataset of +/-80 co-crystals along with a new vision on DRS data analysis. Results confirm that the 'dihedral angle'-rule should be revised. Hydrogen bonding can lead to a more pronounced keto-character, switching off photochromism. The enol-character can indeed be favoured by lowering the amount of intermolecular contacts.